C. R. Mecanique 343 (2015) 199–209

Contents lists available at ScienceDirect

Comptes Rendus Mecanique

www.sciencedirect.com

Numerical limit analysis and plasticity criterion of a porous Coulomb material with elliptic cylindrical voids

Franck Pastor [a], Joseph Pastor [b], Djimedo Kondo [c,*]

[a] Athénée royal Victor-Horta, rue de la Rhétorique, 16, Bruxelles, Belgium
[b] Laboratoire LOCIE, UMR 5271 CNRS, Université de Savoie, 73376 Le Bourget-du-Lac, France
[c] Institut Jean-Le-Rond-D'Alembert, UMR 7190 CNRS, UPMC, 75252 Paris cedex 05, France

ARTICLE INFO

Article history:
Received 12 October 2014
Accepted 8 December 2014
Available online 31 January 2015

Keywords:
Gurson-type models
Cylindrical voids
Porous Coulomb material
Micromechanics
Limit analysis
Static and mixed methods
Conic programming

ABSTRACT

The paper is devoted to a numerical Limit Analysis of a hollow cylindrical model with a Coulomb solid matrix (of confocal boundaries) considered in the case of a generalized plane strain. To this end, the static approach of Pastor et al. (2008) [18] for Drucker–Prager materials is first extended to Coulomb problems. A new mixed—but rigorously kinematic—code is elaborated for Coulomb problems in the present case of symmetry, resulting also in a conic programming approach. Owing to the good conditioning of the resulting optimization problems, both methods give very close bounds by allowing highly refined meshes, as verified by comparing to existing exact solutions. In a second part, using the identity of Tresca (as special case of Coulomb) and von Mises materials in plane strain, the codes are used to assess the corresponding results of Mariani and Corigliano (2001) [13] and of Madou and Leblond (2012) [11] for circular and elliptic cylindrical voids in a von Mises matrix. Finally, the Coulomb problem is investigated, also in terms of projections on the coordinate planes of the principal macroscopic stresses.

1. Introduction

In his celebrated paper [1], Gurson has given an approximate expression of the plasticity criterion of porous materials based on the consideration of a hollow von Mises sphere or cylinder and on the kinematic method of the Limit Analysis (LA) theory. Recent studies were devoted to porous materials with a matrix exhibiting a pressure-sensitive behavior ([2–4], etc.). Other extensions of the Gurson model accounting for void-shape effects have been also proposed: see among others the references [5–10] for spheroidal voids, and [11,12] for ellipsoidal cavities.

In the case of cylindrical cavities with circular or elliptic cross-sections, up to our knowledge, in the literature only exist the theoretical studies of [13] and [11] for porous materials with von Mises matrix. From the numerical point of view, the static and kinematic methods of LA have been elaborated for Gurson problems, i.e. a von Mises matrix with cylindrical cavities, in the references [14–16], and [17]. A first attempt to extend these works for pressure-dependent criteria was presented in [18] for porous Drucker–Prager materials under a generalized plane strain. Analogous studies for porous Tresca–Coulomb materials with cylindrical voids have not been considered in the literature, no more than theoretical investigations, up to our knowledge.

* Corresponding author.
E-mail addresses: F.pastor@skynet.be (F. Pastor), joseph.pastor@univ-savoie.fr (J. Pastor), djimedo.kondo@upmc.fr (D. Kondo).

http://dx.doi.org/10.1016/j.crme.2014.12.004
1631-0721/

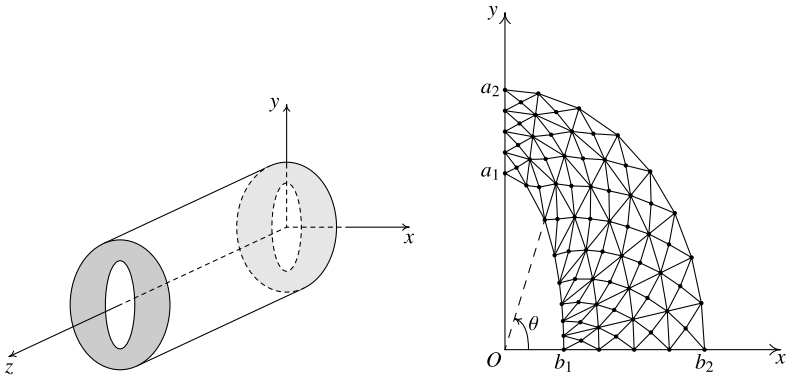

Fig. 1. The hollow cylinder model ($a_1/b_1 = 3$, $f = 0.2$).

Therefore, the main purpose of the present paper is to provide lower and upper bounds to be used as reference values for forthcoming attempts to determine approximate criteria for porous Tresca–Coulomb materials with circular and elliptic cylindrical cavities. An example of the usefulness of these bounds can be found in a recent paper [19], where the previous numerical results of [4] were used for comparison and validation of the proposed estimates for the macroscopic criterion.

The paper is organized as follows. First, we briefly present the hollow cylindrical problem and its formulation in terms of limit analysis. Then, we recall, briefly, the limit analysis methods used here, and the corresponding expressions needed to assess the result through a complete post-analysis of the optimal fields. The next step is devoted to detail the proposed numerical formulation for the mixed (but rigorously kinematic) method, focusing on the case of the generalized plane strain, since it is the first time that the LA mixed approach is applied to mechanical problems in this case of symmetry.

Taking advantage of the identity of Tresca and von Mises materials in plane strain, the static and kinematic codes are firstly validated by comparison with the Gurson exact solution to the hollow cylinder model under transverse isotropic loadings. In a second step, for these materials and for circular and elliptic cylindrical problems, the codes are used to assess the available results of [13] and [11] in terms of projections on the coordinate planes of the macroscopic principal stresses. Finally, the Coulomb problem is investigated, also for circular and elliptic cross-sections of the cylindrical void.

2. The hollow cylinder model

The hollow cylinder model is made up of an elliptic cylindrical cavity embedded in a cylinder with a confocal boundary. The solid matrix is an isotropic, homogeneous and rigid-plastic Coulomb material, with the Tresca material as a special case. Fig. 1 presents the geometric model, where the given aspect ratio a_1/b_1 and porosity f allow us to determine the parameters a_2 and b_2 of the confocal elliptic boundary.

In the generalized plane strain problem, the stress tensor σ and the strain rate tensor d do not depend on the coordinate z. Let us note Σ and D the macroscopic stress and strain rate tensors; these quantities are related to the local fields by the averages over the cross-section S of the model in the plane (x, y):

$$\Sigma_{ij} = \frac{1}{S}\int_S \sigma_{ij}\,\mathrm{d}S; \qquad D_{ij} = \frac{1}{S}\int_{\partial S}\frac{1}{2}(u_i n_j + u_j n_i)\,\mathrm{d}(\partial S) \tag{1}$$

where u denotes the velocity vector and n the (outward) normal unit vector to the boundary ∂S of the model.

More precisely, the local velocity vector u is defined by the components $u_x(x, y), u_y(x, y), u_z = D_z z$, so that the axis z is a principal axis for both tensors. This is a special case of the general 3D-plane problem proposed in [20] from specific periodicity considerations, recently used in [21], among others.

Under the uniform strain rate boundary conditions, i.e. $u_i = D_{ij}x_j$ (in which x represents the position vector), on the outer boundary ∂S, the overall virtual dissipated power P_{tot} can be written as follows:

$$P_{\mathrm{tot}} = S\,Q \cdot q \tag{2}$$

where the loading vector Q and the generalized velocity q are defined as:

$$Q_1 = \Sigma_x, \quad Q_2 = \Sigma_y, \quad Q_3 = \Sigma_z, \quad Q_4 = \Sigma_{yz}, \quad Q_5 = \Sigma_{zx}, \quad Q_6 = \Sigma_{xy}$$
$$q_1 = D_x, \quad q_2 = D_y, \quad q_3 = D_z, \quad q_4 = 2D_{yz}, \quad q_5 = 2D_{zx}, \quad q_6 = 2D_{xy}$$

From the matrix isotropy and the elliptic cross-section of the model, the resulting material is orthotropic with the axis z as one anisotropy axis, becoming transversally isotropic around this axis for circular cross-sections. Here the macroscopic criterion $g(\Sigma)$ is investigated in the $(Oxyz)$ anisotropy frame in terms of projection on the loading planes. For example, we search for the projection of $g(\Sigma)$ in the (Q_1, Q_2) plane by optimizing Q_2 for fixed Q_1, the other loading components being

free. Hence, $\frac{\partial g}{\partial \Sigma_{ij}} = 0 = 2D_{ij}$ for $i \neq j$, and $\frac{\partial g}{\partial Q_3} = 0 = q_3$, since the macroscopic material complies to the normality rule. The same reasoning holds when considering the projections in the other planes (Q_2, Q_3) and (Q_1, Q_3).

Finally, loadings can be restricted to principal components of the macroscopic strain rates D, as well as those of Σ since $(Oxyz)$ is an orthotropic anisotropy frame. Therefore, the quarter of the hollow cross-section is meshed into discontinuous triangular elements, as shown in Fig. 1 (right).

Due to the bad conditioning of the classic kinematic approach experienced for porous Drucker–Prager materials in [18] (where the usual allowed number of elements was 672...), we have elaborated a new mixed kinematic approach based on affine velocity fields in the triangle elements (Lagrange P1). Another motivation to do this was induced by the high level of performance allowed by the mixed approach for the hollow spheroid problems investigated in [22] and [23]. Such level of performance will be verified in the following tests, resulting in lower and upper bounds almost undistinguishable (*a posteriori* verified) obtained in a couple of seconds for each point on a laptop computer.

3. LA methods and Coulomb criterion

The purpose of the limit analysis theory is to determine the locus of the limit loads that corresponds to the macroscopic plasticity criterion searched for in the present hollow cylinder problem. Classically, the limit loads can be determined by using the static (lower bound) method and the kinematic (upper bound) method. The present static approach is carried out by means of an extension of the generalized plane strain code of [18] from the Drucker–Prager to the Coulomb material by using the formulation of the plasticity criterion proposed further. For the sake of homogeneity, we focus here only on the mixed formulation, which is fully novel.

3.1. The mixed kinematic method

The so-called mixed formulation was pioneered by Anderheggen and Knopfel [24] for finite-element models with continuous velocities and a linearized von Mises criterion. An extension to the discontinuous velocity case, based on the assumption that linear programming duality properties remain valid in non-linear programming, was proposed in [25]. A general extension—without any *a priori* assumption—to the discontinuous case using convex optimization was successfully experienced in [26] and [27] for homogeneous von Mises and Gurson materials in plane strain. This general formulation reads:

$$\max_{Q,\sigma,T'} F = V q_0 \cdot Q \tag{3a}$$

$$\text{s.t.} \quad \int_V d : \sigma \, \mathrm{d}V + \int_{S_{\text{disc}}} [u] \cdot T' \, \mathrm{d}S = V q(u) \cdot Q \quad \forall \, \text{KA } u \tag{3b}$$

$$f(\sigma) \leq 0, \qquad f_{nt}\left(T'\right) \leq 0 \tag{3c}$$

where d is the strain rate tensor, σ the stress tensor, V the volume of the mechanical system, S_{disc} the union of the velocity discontinuity surfaces (which are here the inter-element sides of the finite-element mesh), T' the stress vector on these surfaces and $f_{nt}(T')$ the projection of $f(\sigma')$ on the Mohr plane associated with the discontinuity surface of normal n. In (3), the velocity field u must be kinematically admissible (KA), i.e. the velocity u is piecewise continuous with bounded discontinuities $[u]$, and verifies the boundary conditions. Studies in [26] and [27] have demonstrated that the optimal velocity field will also be plastically admissible (PA), i.e. there exists a tensor σ or a vector T' that are respectively associated with the strain rate tensor or to the velocity jump by the normality law corresponding to $f(\sigma) = 0$ and $f_{nt}(T') = 0$.

The previous formulation gives the exact solution if all velocity and stress fields could be taken into account. In general, this is not the case when we consider a discretization of the mechanical system in finite elements. However, the following formulation preserves the upper bound character of the solution from the convexity of the sets of the strain rate tensors and of the velocity jumps plastically admissible, together with the convexity of the unit dissipated powers.

3.2. The Coulomb criterion

The original Coulomb criterion reads:

$$f(\sigma) = |\sigma_i - \sigma_j| - 2c\cos\phi + (\sigma_i + \sigma_j)\sin\phi \leq 0 \tag{4}$$

where σ_i and σ_j are the principal stresses ($i, j = 1, 2, 3$, $i \neq j$), c is the cohesion of the material and ϕ the internal friction angle. Taking into account that σ_z is a principal stress in the present study, the criterion (4) reads:

$$\begin{cases} \sqrt{(\sigma_x-\sigma_y)^2+4\tau_{xy}^2} \le U \\ U \le -\alpha\sin\phi + 2c\cos\phi \\ U \le -\left(\alpha - 2\sigma_z\dfrac{1-\sin\phi}{1+\sin\phi}\right) + 4c\dfrac{\cos\phi}{1+\sin\phi} \\ U \le \left(\alpha - 2\sigma_z\dfrac{1+\sin\phi}{1-\sin\phi}\right) + 4c\dfrac{\cos\phi}{1-\sin\phi} \end{cases} \tag{5}$$

with $\alpha = \sigma_x + \sigma_y$.

In the Mohr plane related to a velocity discontinuity facet of normal n, the Coulomb criterion reads:

$$f_{nt}(T) = |\sigma_{nt}| + \sigma_n\tan\phi - c \le 0 \tag{6}$$

Let us recall the condition of plastic admissibility for the strain rate, and the expression of the volumic dissipated power [28]:

$$\big(|d_1|+|d_2|+|d_3|\big)\sin\phi \le \operatorname{tr}(d); \qquad \pi_{\text{vol}}(d) = \frac{c}{\tan\phi}\operatorname{tr} d \tag{7}$$

where d_1, d_2 and d_3 are the principal strain rates. From (7), the domain of the PA strain rates is a convex cone whose apex corresponds to the null tensor.

The corresponding relations about the velocity discontinuities read:

$$\big|[u_t]\big|\tan\phi \le [u_n]; \qquad \pi_{\text{disc}}\big([u]\big) = c\frac{[u_n]}{\tan\phi} = c\big|[u_t]\big| \tag{8}$$

The expressions (7) and (8) here are only used in the post-analysis of the optimal solution to the mixed method. Note that a common formulation for Tresca (i.e. Coulomb with $\phi = 0$) and Coulomb materials can be easily obtained by introducing the non-negative auxiliary variables Y and Z and the two following equalities:

$$\operatorname{tr}(d) = Y\sin\phi; \qquad [u_n] = Z\tan\phi \tag{9}$$

Using these variables, the dissipated powers in (7) and (8) become linear in Y and Z, respectively, giving rise to an unique classic kinematic code that was used for validation for the mixed approach with slightly refined meshes. As mentioned before, we detail only the formulation of the mixed approach in the following.

4. Numerical implementation of the mixed method

Fig. 1 (right) illustrates the case of a mesh with n_l $(=4)$ layers, n_s $(=8)$ angular sectors and $n_l \times n_s \times 4$ triangles. For each aspect ratio a_1/b_1 of the cavity and for a given porosity, the elliptic boundary of the mesh is computed to obtain its confocal form. Since these boundaries are not homothetic when the aspect ratio is not equal to 1, the porosity after meshing is not exactly the input one. Therefore, in a first step for each case of porosity and aspect ratio, the distribution of the angle θ is optimized to obtain the desired porosity by progressively concentrating this distribution towards the more curved boundary zone.

4.1. The virtual velocity field

In each Lagrange P1 triangle, the displacement velocity in the plane is affine and defined by the six "nodal" velocities u_x and u_y; it is completed by $u_z = D_z z$ where D_z is a variable common to all triangles.

Then, the strain rate tensor is constant over the triangle.

Along an inter-element side the velocity jump $[u]$ is linear. If the jump is PA at the ends of the side, it will be PA along the side, owing to the convexity of the set of the PA velocity jumps. Moreover, the corresponding dissipated power can be upper bounded by a linear interpolation between its values at the ends of the side. These features will be used in the following in order to preserve the upper bound character of the final solution.

4.2. Formulation of the virtual power principle (3b)

4.2.1. Expression of the external power

A unique stress tensor $\{\sigma\} = (\sigma_x, \sigma_y, \sigma_{xy}, \sigma_z)^{\mathrm{T}}$ is assigned to each triangle. From the two "nodal" components (u_x, u_y) located at each apex of the triangle, the velocity vector at the current point is obtained from the classic interpolation matrices $[N]$. The generalized velocities $(q_1 = D_x, q_2 = D_y, q_3 = D_z)$ are added to the global vector $\{u\}$ in order to form the final virtual vector $\{X\}$. Thus, from (2), the external power can be written as:

$$P_{\text{ext}} = S_t(q\cdot Q) = S_t\{q\}^{\mathrm{T}}\{Q\} = \{X\}^{\mathrm{T}}S_t[\beta]\{Q\} \tag{10}$$

where $\{q\} = [\beta]^{\mathrm{T}}\{X\}$ and S_t the (total) area of the plane model.

4.2.2. Contribution of the element velocity fields

Into the triangular element k, the strain rate $\{d\}$ is defined by:

$$\{d\} = (d_x, d_y, 2_{dxy}, d_z)^{\mathrm{T}} = \begin{Bmatrix} [B]_k\{u^n\} \\ D_z \end{Bmatrix} \tag{11}$$

where $[B]$ is the classic plane strain matrix defined from the interpolation matrices. Let us numerically write the virtual power principle (3b) as:

$$-\sum_k S_k\{d\}_k^{\mathrm{T}}\{\sigma\} + \{X\}^{\mathrm{T}} S_{\mathrm{t}}[\beta]\{Q\} = 0 \quad \forall\{X\}\ \mathrm{KA} \tag{12}$$

where k refers to the current element of surface S_k. Using Eq. (11) and after assembling the elements, the relationship (12) gives rise to the following variational system:

$$\{X\}^{\mathrm{T}}\big[-[\alpha]\{\sigma\} + S_{\mathrm{t}}[\beta]\{Q\}\big] = 0 \quad \forall\{X\}\ \mathrm{KA} \tag{13}$$

where the matrix $[\alpha]$ results from the assembly of the submatrices $[\alpha]_k = S_k\left[\begin{smallmatrix} [B]_k^{\mathrm{T}} & 0 \\ 0 & 1 \end{smallmatrix}\right]$ defined from (11).

4.2.3. Contribution of the velocity discontinuities

The second part of the integral in (3b) is the sum of the power contribution of each discontinuity line L_{1-2} (of normal n and ends noted 1 and 2):

$$P_{\mathrm{d}} = \int_{L_{1-2}} [u]\cdot T'\,\mathrm{d}l = \int_{L_{1-2}} \big\{[u]\big\}^{\mathrm{t}}\big\{T'\big\}\,\mathrm{d}l \tag{14}$$

According to [28], the product $[u]\cdot T'$ becomes the dissipated power $\pi_{\mathrm{d}}([u])$ (which only depends on $[u]$) when the stress vector T' and the velocity jump vector $[u]$ are associated relatively to the $f_{nt}(T')$ criterion. Then, $[u]$ will be PA along the side if it is PA at its ends, from the linearity of $[u]$ and from the convexity of the set of the PA velocity jumps.

Now, we can use the convexity of $\pi_d([u])$ since $[u]$ vary linearly along the discontinuity side: to the product $\{[u]\}^t\{T'\}$ we substitute its linear interpolation $\mathcal{L}(\{[u]\}^{\mathrm{t}}\{T'\})$ between its values at each end of the discontinuity side. By allocating a stress vector $T' = (\sigma_n, \sigma_{nt})$ expressed in the orthonormal (n,t) frame of the side (without any variation hypothesis along this side) at each end of the discontinuity side L_{1-2}, we finally obtain:

$$P_{\mathrm{d}} \le \frac{l}{2}\sum_{i=1,2} [u]_i^{\mathrm{t}}\big\{T_i'\big\} \tag{15}$$

where l is the length of L_{1-2}. Here $[u_i]$ and T_i' are defined in the local frame (n,t) of the discontinuity. After expressing the velocity jump in terms of the corresponding variables (u_x, u_y), and adding the T_i' as new stress variables, the variational equation (13) can be completed with the additional term $\{X\}^{\mathrm{T}}[\alpha']\{T'\}$.

4.2.4. The PA stress conditions

In the frame (x,y), the Coulomb plasticity criterion is written as in (5), where the cone can be easily cast into the Lorentz form required by the conic optimizer MOSEK [29]:

$$\sqrt{x_1^2 + x_2^2} \le U \tag{16}$$

completed with the three linear inequalities for each triangular element.

The criterion (6) for the stress vector T' gives rise to the two following inequalities:

$$\sigma_{nt}' + \sigma_n' \tan\phi \le c, \qquad -\sigma_{nt}' + \sigma_n' \tan\phi \le c \tag{17}$$

which results in two linear constraints in terms of the real variables σ_{nn}' and σ_{nt}' for each ends of the discontinuity sides.

4.2.5. The final mixed problem and the KA conditions

Finally, the numerical form of the variational mechanical Problem (3) is as following:

$$\begin{aligned} &\mathrm{Max}\ S_{\mathrm{t}}\{q_0\}^{\mathrm{T}}\{Q\} \\ \text{s.t.}\quad &-[\alpha]\{\sigma\} - \big[\alpha'\big]\big\{T'\big\} + S_{\mathrm{t}}[\beta]\{Q\} = 0 \\ &f(\sigma) \le 0 \quad \forall\sigma; \qquad f_{nt}\big(T'\big) \le 0 \quad \forall T' \\ &+\ \mathrm{KA\ conditions} \end{aligned} \tag{18}$$

Table 1
Comparison to Σ_h exact values—circular cylindrical void—porosity $f = 0.2$—$c = 1$, $\phi = 0$.

n_l, n_s	12–12	24–24	48–48	72–72	96–96
Gurson value	1.609438	1.609438	1.609438	1.609438	1.609438
Mixed kine.	1.612069	1.610099	1.609604	1.609513	1.609480
CPU time/s	< 1	< 1	2	10	15
Static	1.592837	1.60486	1.605847	1.606814	1.608126
CPU time/s	< 1	1	3	9	22

Table 2
Evolution of the power dissipated on the discontinuities relatively to the total one with the mesh refinement.

n_l, n_s	12–12	24–24	48–48	72–72	96–96	120–120
P_{disc}/P_{tot}	$2.57{\cdot}10^{-3}$	$3.88{\cdot}10^{-4}$	$1.00{\cdot}10^{-4}$	$4.93{\cdot}10^{-5}$	$2.92{\cdot}10^{-5}$	$2.02{\cdot}10^{-5}$

As shown in the detailed analysis of [26] and [23], we can identify the dual variables (associated with the rows of the constraint matrix) of the optimal solution to the problem with the components of $\{X\}$. This analysis also detailed how the resulting velocity field is plastically admissible and how, by adding auxiliary columns, the kinematically admissible character of the optimal velocity field can be ensured. Here, the KA conditions are formulated as in the following.

- We previously defined three supplementary rows (constraints) whose associated virtual variables are q_1, q_2 and q_3, and three new columns for the macroscopic stresses Q_1, Q_2 and Q_3. At each apex of the triangle sides of the boundary, the loading conditions $u_x = D_x x$ and $u_y = D_y y$ are imposed. This is done by adding one additional column (i.e, an additional variable) for each of these conditions. For example, the terms of the condition $u_x - xD_x = 0$ are dispatched on the corresponding components u_x and D_x $(= q_1)$ in the additional column. No supplementary condition is needed for imposing $q_i = q_{0_i}$, since this results from the optimality conditions as detailed in [23].
- A similar technique is used to impose the null symmetry value to the u_y components on the x axis, and to the u_x components on the y axis.
- As in the static approach, additional constraints can be added in the mixed approach in order to impose linear relations between the loadings Q_i, since they are real variables of the problem.

5. Numerical tests and evaluation of existing macroscopic criteria

5.1. Comparison with exact results for circular cylindrical voids

For cylindrical voids, the Gurson criterion is exact in the loading case $\Sigma_x = \Sigma_y$. From the identity of von Mises and Tresca materials in plane strain, the present results can be compared to these exact solutions when maximizing $\Sigma_h = (\Sigma_x + \Sigma_y)/2$ for $\Sigma_x = \Sigma_y$. In Table 1, one can see that not only the numerical upper bounds are very close to the exact ones, but also the CPU times are very small. The code was run on an Apple Mac Book Pro with 16 gigabytes of RAM and a 2.7 GHz Core i7 with 4 cores. To be complete, we have given also the results of the modified static code in order to obtain the lower bounds for the same meshes.

With the 96–96 mesh, the numerical problem involves 36,864 triangles, 625,923 linear constraints, 36,864 cones, and 479,235 variables. For the corresponding static approach, one has: 36,864 triangles, 847,878 linear constraints, 110,592 cones, and 847,878 variables. In both cases, the problem has been solved using the release 5 of the conic code MOSEK [29]. From the results of Table 1, all verified *a posteriori*, it can be concluded that the mixed kinematic approach and the static code have now the same level of efficiency. Moreover, they require very little computation time, due to the performance of the conic optimizer, this performance being also linked to the very good conditioning of the numerical problems addressed here.

An interesting question arises about the role of the velocity discontinuities when refining the mesh. It can be seen in Table 2 that their contribution to the total dissipated power is lowering (but never becoming zero), as expected since the set of the numerical velocity fields becomes large enough to obtain precise results with less benefit induced by the discontinuities. Nevertheless, a specific comparison with an *ad hoc* modified code without discontinuities should be interesting, but out of the scope of the present paper.

5.2. Comparison with previous results in plane strain—Tresca/von Mises matrix

As mentioned before, the macroscopic criterion is investigated in terms of projections on the coordinate planes of the principal frame $(\Sigma_x, \Sigma_y, \Sigma_z)$ (which is also here the principal frame (D_x, D_y, D_z)). Consequently, when considering the projection on the plane (Σ_i, Σ_j), the component D_k, with $i, j \neq k$, is assigned to zero. This natural choice, allowed by

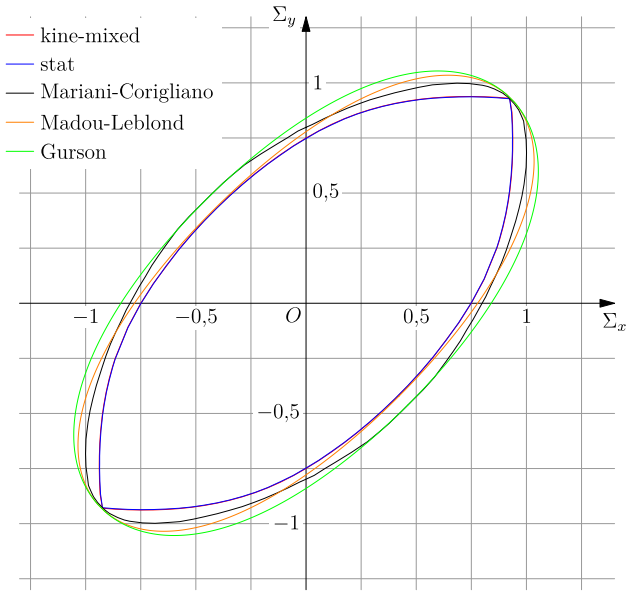

Fig. 2. (Color online.) Tresca/von Mises matrix—static (blue)/kinematic (red) results versus Gurson (green), Madou and Leblond (orange) Mariani and Corigliano (black) criteria—circular void—$D_z = 0$—$f = 0.2$—$a_1/b_1 = 1$—$\phi = 0$—$c = 1$.

the optimization nature of the numerical problems, is also motivated for facilitating the following comparisons with the corresponding results of [13].

5.2.1. Circular cylindrical void

Using here also the identity of von Mises and Tresca materials in plane strain, we can now compare to the corresponding results given by Gurson [1], Madou and Leblond [11], Mariani and Corigliano [13] for the hollow cylinder problem with a von Mises matrix. Madou and Leblond provide also a closed form expression that reads, taking into account that the present loading Σ is principal:

$$\frac{\Sigma_{eq}^2}{\sigma_0^2} + 3f\frac{(\Sigma_x - \Sigma_y)^2}{\sigma_0^2} + 2f\cosh\left(\frac{\sqrt{3}}{2}\frac{\Sigma_x + \Sigma_y}{\sigma_0}\right) - 1 - f^2 = 0 \tag{19}$$

where $\sigma_0 = c\sqrt{3}$. From the plane strain hypothesis, we can specialize (19) by using $\Sigma_z = (\Sigma_x + \Sigma_y)/2$ and $\Sigma_{eq}^2 = 3(\Sigma_x - \Sigma_y)^2/4$. When $\Sigma_x = \Sigma_y$, Expression (19) becomes the Gurson criterion, which is an exact solution in this case. To compare to the Mariani–Corigliano criterion, we have scanned the corresponding curves in [13] (Fig. 2a, $E_{33} = E_z = 0$) by using the open source Java program Plotdigitizer (http://plotdigitizer.sourceforge.net/). All these curves (normalized by the cohesion c) are plotted in Fig. 2.

Several comments can be made from these graphs. The static and the kinematic bounds are almost indistinguishable, and always in the good order, as it can be verified by zooming on the figure. This closeness confirms the angular point on the $(\Sigma_x + \Sigma_y)$ axis pointed out in [14,17] and illustrated in [16]; in this paper, Fig. 4 gives the optimal generalized velocity vectors q at the vicinity of the corner point, in the frame (Q1, Q2) selected in this work, i.e. $Q_1 = (\Sigma_x + \Sigma_y)/2$ and $Q_2 = (\Sigma_x - \Sigma_y)\sqrt{3}/2$. It is confirmed in Fig. 2 of the present paper, with now a very fine precision, that the macroscopic criterion presents a corner on the isotropic axis where $\Sigma_x = \Sigma_y$; this corner induces a cone of admissible $(D_x, D_y, D_z = 0)$, this cone including the case $D_x = D_y$, the existence of which, but not its unicity, is imposed from symmetry considerations. Taking into account that the present results are general, *a posteriori* controlled bounds, the presence of this corner cannot be an effect of the numerical aspect of the methods; a physical origin cannot easily be invoked, except, perhaps, if we consider that the von Mises and Tresca matrices are limit cases of Drucker–Prager and Coulomb materials, both criteria exhibiting *a priori* corners on the isotropic axis.

Finally, all the criteria coincide on this isotropic loading axis, as expected because of the exact nature of the solution in this case. The Madou–Leblond and Mariani–Corigliano criteria alternately improve the Gurson values, the first one becoming tangent to the kinematic/static curve near the $(\Sigma_x - \Sigma_y)$ axis.

5.2.2. Elliptic cylindrical void

First, let us note that the results obtained for a given a_1/b_1 hold also for b_1/a_1 by simply inverting Σ_x and Σ_y, owing to the characteristics of the mechanical problem here investigated. Fig. 3 compares the numerical bounds, almost indistinguishable again, with the projection results (in black) of Mariani and Corigliano (Fig. 2b in [13]) for an elliptic cross-section.

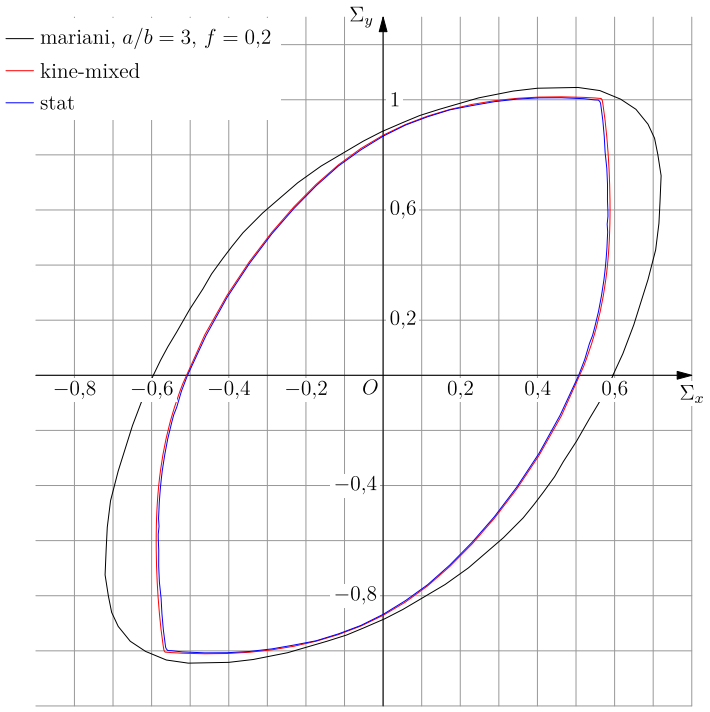

Fig. 3. (Color online.) Tresca/von Mises matrix–static/kinematic results versus Mariani and Corigliano criterion–elliptic void–$f = 0.2$–$a_1/b_1 = 3$–$\phi = 0$–$c = 1$.

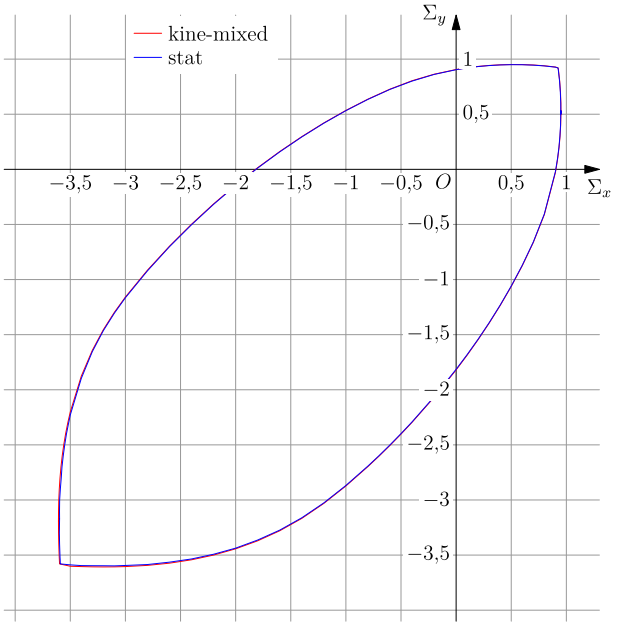

Fig. 4. (Color online.) Coulomb matrix–static/kinematic results–circular void–$f = 0.2$–$a_1/b_1 = 1$–$\phi = 20$–$c = 1$.

Here also the black curve has been obtained with the above-mentioned digitizer. As expected, the graphs do not present any symmetry around the axis of the figure, no more than around the axes $(\Sigma_x + \Sigma_y)$ and $(\Sigma_x - \Sigma_y)$. Let us note that this problem was also studied in [30] with a von Mises matrix, but not in the plane strain case, so that the comparison with the present Tresca study would not be pertinent.

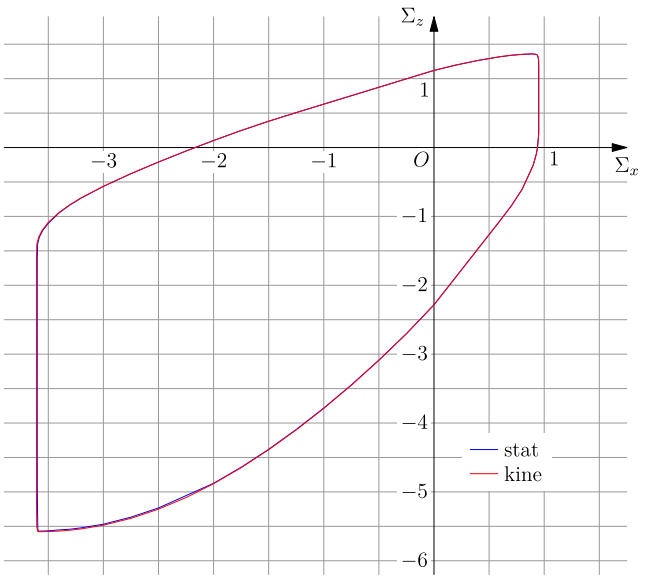

Fig. 5. (Color online.) Coulomb matrix–static/kinematic results–circular void– $f = 0.2$–$a_1/b_1 = 1$–$\phi = 20$–$c = 1$.

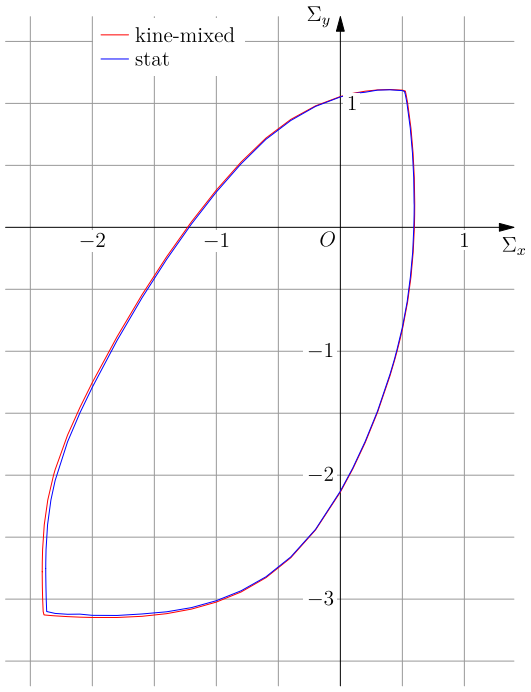

Fig. 6. (Color online.) Coulomb matrix–static/kinematic results–elliptic void– $f = 0.2$–$a_1/b_1 = 3$–$\phi = 20$–$c = 1$.

5.3. Case of a Coulomb matrix

As mentioned above, we search for projections of the macroscopic criterion on the three loading planes.

5.3.1. Circular cylindrical void

Owing to the transverse isotropy of the model, only two projections are needed, i.e. on the plane (Σ_x, Σ_y) given in the Fig. 4, and in the plane (Σ_x, Σ_z) of Fig. 5 for example: the projections on the planes (Σ_x, Σ_z) and (Σ_y, Σ_z) are identical. It can be noticed that static and kinematic results remain remarkably close, and they are symmetric around the (transverse) isotropic loading axis in Fig. 4.

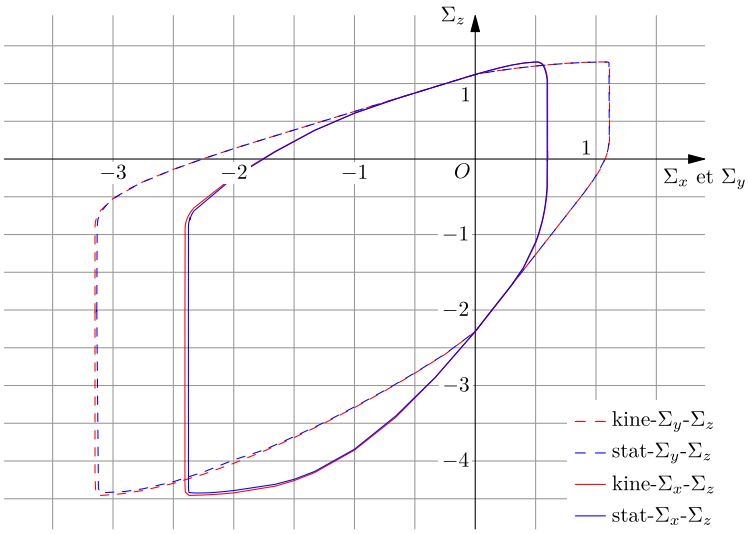

Fig. 7. (Color online.) Coulomb matrix—static/kinematic results—elliptic void—$f = 0.2$—$a_1/b_1 = 3$—$\phi = 20$—$c = 1$.

5.3.2. Elliptic cylindrical void

First, the projections on the (Σ_x, Σ_y) plane: the static (blue) and kinematic (red) bounds are plotted in Fig. 6. For the two other loading planes (Fig. 7), the projections on the plane (Σ_y, Σ_z) are plotted in dashed lines, and the projections on the plane (Σ_x, Σ_z) in solid lines. Here also, the respective lower and upper bounds remain very close, slightly less in the more compressive zone. Fig. 7 (and Fig. 5) presents remarkable vertical lines, this probably being induced by the specific nature of the Coulomb criterion where the intermediate principal stress has no influence on the plasticity criterion.

6. Conclusion

The main purpose of the present paper was to provide numerical, but rigorous bounds to the macroscopic criterion of a "porous Coulomb material" with cylindrical voids, such problem not studied in the literature, at least up to our knowledge. To do this, an original mixed approach, rigorously kinematic, has been developed resulting in a very performant upper bound code whose efficiency has allowed us to use highly refined meshes. This confirms the observations about the mixed approach compared to the classic one, for other matrix materials, in previous works for spherical and oblate cavities. It is worth also noting that the mixed approach was not used up to now in the literature in the case of symmetry considered in the present paper.

The resulting bounds (always controlled *a posteriori*) appear almost indistinguishable in the tests, giving then a quasi-exact approach to the macroscopic criterion of the "porous material", owing to the now common efficiency of the mixed and static codes. Moreover, only a couple of seconds of CPU times is needed to obtain a point of the graph on a recent laptop computer. These bounds, not only allow us to understand and characterize the macroscopic plastic properties of the above class of materials, but are also expected to serve as reference results for forthcoming theoretical investigations.

References

[1] A.L. Gurson, Continuum theory of ductile rupture by void nucleation and growth—part I: yield criteria and flow rules for porous ductile media, J. Eng. Mater. Technol. 99 (1977) 2–15.
[2] J. Lee, J. Oung, Yield functions and flow rules for porous pressure-dependent strain-hardening polymeric materials, J. Appl. Mech. 67 (2000) 288–297.
[3] T.F. Guo, J. Faleskog, C.F. Shih, Continuum modeling of a porous solid with pressure sensitive dilatant matrix, J. Mech. Phys. Solids 56 (2008) 2188–2212.
[4] P. Thoré, F. Pastor, J. Pastor, Hollow sphere models, conic programming and third stress invariant, Eur. J. Mech. A, Solids 30 (2011) 63–71.
[5] M. Gologanu, J. Leblond, Approximate models for ductile metals containing non-spherical voids—case of axisymmetric prolate ellipsoidal cavities, J. Mech. Phys. Solids 41 (11) (1993) 1723–1754.
[6] M. Gologanu, J. Leblond, G. Perrin, J. Devaux, Approximate models for ductile metals containing non-spherical voids—case of axisymmetric oblate ellipsoidal cavities, J. Eng. Mater. Technol. 116 (1994) 290–297.
[7] M. Garajeu, P. Suquet, A micromechanical approach of damage in viscoplastic materials by evolution in size, shape and distribution of voids, Comput. Methods Appl. Mech. Eng. 183 (2000) 223–246.
[8] V. Monchiet, E. Charkaluk, D. Kondo, An improvement of Gurson-type models of porous materials by using Eshelby-like trial velocity fields, C. R. Mecanique 335 (2007) 32–41.
[9] V. Monchiet, O. Cazacu, E. Charkaluk, D. Kondo, Macroscopic yield criteria for plastic anisotropic materials containing spheroidal voids, Int. J. Plast. 24 (2008) 1158–1189.
[10] V. Monchiet, E. Charkaluk, D. Kondo, Macroscopic yield criteria for ductile materials containing spheroidal voids: an Eshelby-like velocity fields approach, Mech. Mater. 72 (2014) 1–18.
[11] K. Madou, J.-B. Leblond, A Gurson-type criterion for porous ductile solids containing arbitrary ellipsoidal voids—II: determination of yield criterion parameters, J. Mech. Phys. Solids 60 (2012) 1037–1058.

[12] K. Madou, J.-B. Leblond, A Gurson-type criterion for porous ductile solids containing arbitrary ellipsoidal voids—I: limit-analysis of some representative cells, J. Mech. Phys. Solids 60 (2012) 1020–1036.
[13] S. Mariani, A. Corigliano, Anisotropic behavior of porous, ductile media, Int. J. Solids Struct. 38 (2001) 2427–2451.
[14] H. Thai-The, P. Francescato, J. Pastor, Limit analysis of unidirectional porous media, Mech. Res. Commun. 25 (1998) 535–542.
[15] P. Francescato, J. Pastor, B. Riveill-Reydet, Ductile failure of cylindrically porous materials—part I: plane stress problem and experimental results, Eur. J. Mech. A, Solids 23 (2004) 181–190.
[16] J. Pastor, P. Francescato, M. Trillat, E. Loute, G. Rousselier, Ductile failure of cylindrically porous materials—part II: other cases of symmetry, Eur. J. Mech. A, Solids 23 (2004) 191–201.
[17] J. Pastor, P.P. Castaneda, Yield criteria for porous media in plane strain: second-order estimates versus numerical results, C. R. Mecanique 330 (2002) 741–747.
[18] F. Pastor, P. Thoré, E. Loute, J. Pastor, M. Trillat, Convex optimization and limit analysis: application to Gurson and porous Drucker–Prager materials, Eng. Fract. Mech. 75 (2008) 1367–1383.
[19] A. Benallal, R. Desmorat, M. Fournage, An assessment of the role of the third stress invariant in the Gurson approach for ductile fracture, Eur. J. Mech. A, Solids 47 (2014) 400–414.
[20] P. Francescato, J. Pastor, Lower and upper numerical bounds to the off-axis strength of unidirectional fiber-reinforced composites by limit analysis methods, Eur. J. Mech. A, Solids 16 (1997) 213–234.
[21] M. Gueguin, G. Hassen, P. de Buhan, Numerical assessment of the macroscopic strength criterion of reinforced soils using semidefinite programming, Int. J. Numer. Methods Eng. 99 (2014) 522–541.
[22] F. Pastor, J. Pastor, D. Kondo, Limit analysis and lower/upper bounds to the macroscopic criterion of Drucker–Prager materials with spheroidal voids, C. R. Mecanique 342 (2014) 96–105.
[23] F. Pastor, D. Kondo, J. Pastor, 3D-FEM formulations of limit analysis methods for porous pressure-sensitive materials, Int. J. Numer. Methods Eng. 95 (2013) 847–870.
[24] E. Anderheggen, H. Knopfel, Finite element limit analysis using linear programming, Int. J. Solids Struct. 8 (1972) 1413–1431.
[25] K. Krabbenhoft, A. Lyamin, M. Hijaj, S. Sloan, A new discontinuous upper bound limit analysis formulation, Int. J. Numer. Methods Eng. 63 (2005) 1069–1088.
[26] F. Pastor, Résolution par des méthodes de point intérieur de problèmes de programmation convexe posés par l'analyse limite, Thèse de doctorat, Facultés universitaires Notre-Dame de la Paix, Namur, 2007.
[27] F. Pastor, E. Loute, J. Pastor, M. Trillat, Mixed method and convex optimization for limit analysis of homogeneous Gurson materials: a kinematical approach, Eur. J. Mech. A, Solids 28 (2009) 25–35.
[28] J. Salençon, Calcul à la Rupture et Analyse Limite, Presses des Ponts et Chaussées, Paris, 1983.
[29] MOSEK ApS, C/O Symbion Science Park, Fruebjergvej 3, Box 16, 2100 Copenhagen ϕ, Denmark, http://www.mosek.com (2010).
[30] K. Madou, Contribution à l'étude des effets de forme des cavités en rupture ductile des métaux, Thèse de doctorat, Université Paris-6, 2012.